Rotational Spectra of the Xe−$(H_2O)_2$ van der Waals Trimer: Xenon as a Probe of Electronic Structure and Dynamics

Qing Wen and Wolfgang Jäger*

Department of Chemistry, University of Alberta, Edmonton, Alberta, Canada T6G 2G2

Received: September 28, 2006; In Final Form: January 17, 2007

Rotational spectra of three isotopomers of the Xe−$(H_2O)_2$ van der Waals trimer were recorded using a pulsed-nozzle, Fourier transform microwave spectrometer. Nine [nine, four] *a*-type and twelve [eleven, seven] *b*-type transitions were measured for the ^{132}Xe−$(H_2O)_2$ [^{129}Xe−$(H_2O)_2$, ^{131}Xe−$(H_2O)_2$] isotopomer. The determined rotational and centrifugal distortion constants were used to extract information about the structure and vibrational motions of the complex. The nuclear quadrupole hyperfine structures due to the ^{131}Xe (nuclear spin quantum number $I = {}^3/_2$) nucleus were also detected. The large value of the off-diagonal nuclear quadrupole coupling constant χ_{ab} in particular provides detailed insight into the electronic environment of the xenon atom and the orientations of the water molecules within the complex. An effective structure that best reproduces the experimental ^{131}Xe nuclear quadrupole coupling constants is rationalized by ab initio calculations. An overall goal of this line of work is to determine how the successive solvation of a xenon atom with water molecules affects the xenon electron distribution and its intermolecular interactions. The results may provide molecular level interpretations of ^{129}Xe NMR data from, for example, imaging experiments.

Introduction

Xenon is a sensitive atomic probe for a variety of in vivo studies using nuclear magnetic resonance (NMR) and magnetic resonance imaging (MRI) methods. High-spin polarization of ^{129}Xe (nuclear spin quantum number $I = {}^1/_2$) can be achieved with an optical pumping scheme and significantly enhances sensitivity and contrast of these experiments.[1] Such hyperpolarized ^{129}Xe has been utilized to obtain high-resolution images of void spaces in the body, for example, human lungs.[3] These high-resolution images are usually difficult to obtain by conventional X-ray and ^{1}H MRI methods because of low concentrations of signal sources in the gas phase. Today, the MRI method has evolved to be an indispensable tool for the investigation, diagnosis, and treatment of various pulmonary diseases. In addition to lung images, ^{129}Xe NMR/MRI studies have been extended to blood and various tissues of the body.[4] Such applications have become a very promising method to, for example, characterize the blood flow and to probe brain functions under certain physiological conditions.[5]

The success of xenon in the in vivo NMR/MRI studies can mainly be attributed to its large and easily polarizable electronic structure. Interactions of Xe with its environment have dramatic effects on the electronic properties of the xenon atom and, as a result, directly affect its NMR relaxation parameters, chemical shifts, and the solubility of xenon. Fundamental understanding of the Xe molecule interactions is therefore of great importance for the prediction and molecular level interpretations of ^{129}Xe shielding response in NMR/MRI experiments. Water molecules make up over $^2/_3$ of the mass of the human body, and their interactions with xenon determine the traveling paths of xenon in the body and contribute significantly to background signals of in vivo images. As a result of the hydrophobic Xe−water interaction, a biocompatible gas carrier, for example, the recently reported water soluble Cryptophanes,[6] is necessary to increase the solubility of xenon and to deliver xenon into the target tissues. A detailed characterization of the Xe−water interaction might help to improve hyperpolarized ^{129}Xe in vivo delivery methods and to interpret the results obtained and the phenomena observed in NMR/MRI studies. In addition, detailed knowledge about interactions of xenon with water, a prototypical model of hydrophobic interactions, will contribute to a better understanding of more complex interactions in biological systems. A number of experimental and theoretical NMR studies have been carried out in an attempt to gain insight into this interaction.[7,8] We have recently studied the Xe−H_2O van der Waals dimer using both Fourier transform microwave spectroscopy and ab initio computations.[9] Information about the structure and dynamics of the complex has been extracted from the microwave data with the assistance of an ab initio potential. In this work, we report a microwave spectroscopic study of the Xe−$(H_2O)_2$ trimer. The variation of structure and dynamics in going from the dimer to the trimer are elucidated and interpreted in terms of non-additive three-body effects. The studies of both Xe−H_2O dimer and Xe−$(H_2O)_2$ trimer are stepping stones for understanding how the xenon electron distribution is affected by successive solvation with water molecules.

One other Rg−$(H_2O)_2$ complex, namely, Ar−$(H_2O)_2$, has been previously studied in the microwave region.[10,11] The structure of Ar−$(H_2O)_2$ was described as an isosceles triangle, treating the water molecules as spheres. The experimental results suggest that Ar approaches the water dimer from an axis perpendicular to the plane of the water molecule that acts as a proton donor. The presence of Ar shows little effect on the intermolecular distance in the water dimer. It is instructive to see how the structure and hydrogen bonding interaction of the water dimer will be affected by the larger and more polarizable xenon atom.

* To whom correspondence should be addressed. E-mail: wolfgang.jaeger@ualberta.ca. Phone: 1-780-492-5020. Fax: 1-780-492-8231.

10.1021/jp0663863 CCC: $37.00
Published on Web 02/23/2007

A free xenon atom has a closed electron shell structure and therefore a spherically symmetric electronic charge distribution. This distribution will be distorted by a microscopic environment, for example, surrounding water molecules. The degree of distortion depends uniquely on the type, position, and orientation of its neighbors and can be directly detected by NMR/MRI techniques. Knowledge about how the electronic structure of the xenon atom is affected by the surrounding molecular distribution will therefore be crucial in bridging the gap between the macroscopic phenomena observed in NMR/MRI experiments and their microscopic, molecular level interpretations. This knowledge can be obtained by measuring the ^{131}Xe ($I = {}^3/_2$) nuclear quadrupole hyperfine structures of ^{131}Xe-containing isotopomers. Information about the distortion of the electronic structure of the xenon atom from a spherically symmetric charge distribution can then be extracted from the resulting nuclear quadrupole coupling constants.

In this paper, we present a high-resolution microwave spectroscopic investigation of the Xe−$(H_2O)_2$ complex. Rotational transitions of ^{132}Xe−$(H_2O)_2$, ^{131}Xe−$(H_2O)_2$, and ^{129}Xe−$(H_2O)_2$ were measured using a Fourier transform microwave spectrometer. Nuclear quadrupole hyperfine structures arising from the quadrupolar ^{131}Xe nucleus were detected and analyzed. The spectroscopic results were used to derive information about the structure and the vibrational dynamics of the complex. An effective structure, determined from the ^{131}Xe nuclear quadrupole coupling constants, is rationalized and supported by ab initio computations.

Experimental Details

The rotational spectra of Xe−$(H_2O)_2$ were measured using a pulsed nozzle, Fourier transform microwave spectrometer described previously.[12] The Xe−$(H_2O)_2$ complexes were generated and stabilized in a supersonic expansion of a gas mixture through a General Valve (Series 9) pulsed nozzle with an orifice diameter of 0.8 mm. The molecular expansion traveled parallel to the direction of the microwave propagation, and as a result, all observed transitions were doubled due to the Doppler effect. The gas mixture consisted of 0.15% H_2O vapor and 0.6% Xe in Ne carrier gas at pressures of ∼6 atm. Typical line widths for well-resolved transitions are ∼7 kHz (full width at half-maximum). The measurement accuracy is estimated to be ±1 kHz.

Spectroscopic Search and Assignment

On the basis of the geometry of Ar−$(H_2O)_2$,[10,11] the rotational constants *A*, *B*, and *C* of Xe−$(H_2O)_2$ were predicted by assuming a simple isosceles triangular structure of the trimer with two water spheres and a xenon atom. By use of the structures of the Ar−H_2O,[13] Ar−$(H_2O)_2$,[10,11] and Xe−H_2O (ref 9) complexes as a guide, we estimated the distance from Xe to the center-of-mass (c.m.) of H_2O to be 3.90 Å, and the c.m.(H_2O)−c.m.-(H_2O) distance to be 3.00 Å. With an estimated inertial defect $\Delta = 1.0$ amu Å^2, the *A*, *B*, and *C* rotational constants of ^{132}-Xe−$(H_2O)_2$ were predicted to be 6253, 1377, and 1126 MHz, respectively. These predictions are within 20 MHz of the experimental values determined later in this work.

1. ^{132}Xe−$(H_2O)_2$ and ^{129}Xe−$(H_2O)_2$. Nine [nine] *a*-type and twelve [eleven] *b*-type transitions with rotational quantum number *J* ranging from 0 to 5 and K_a from 0 to 2 were measured for the ^{132}Xe−$(H_2O)_2$ [^{129}Xe−$(H_2O)_2$] isotopomer. All measured transition frequencies are listed in Table S1 of the Supporting Information together with the quantum number assignments. Rotation-tunneling spectra of Xe−$(H_2O)_2$ that could arise from the internal rotation of the H_2O molecules were not observed. In the case of Ar−$(H_2O)_2$,[10,11] two components were detected for each *a*-type transition with tunneling splittings in the range from 50 to 600 kHz. Possible reasons for only one detected component in Xe−$(H_2O)_2$ could be too low a transition intensity (for spin statistical reasons) for the second component to be observed or quenching of the tunneling splitting as a result of the increased angular anisotropy of the Xe−$(H_2O)_2$ potential compared to that of Ar−$(H_2O)_2$. In a number of transitions, we observed narrow splittings of about 20 kHz. The origin of these splittings could be the tunneling motion or proton hyperfine structures arising from H−H spin−spin or H spin−rotation interactions. However, these hyperfine structures could only be partially resolved, and no attempt was made to fit and to interpret them. In those cases, the frequency of the most intense component was recorded as the transition frequency (Table S1 of the Supporting Information). Pickett's SPFIT/SPCAT suite of programs[14] was used to fit spectroscopic constants to measured transition frequencies. The rotational constants *A*, *B*, and *C*, and five quartic centrifugal distortion constants D_J, D_{JK}, D_K, d_1, and d_2 were determined and are given in Table 1.

TABLE 1: Spectroscopic Constants of ^{132}Xe−$(H_2O)_2$, ^{131}Xe−$(H_2O)_2$, and ^{129}Xe−$(H_2O)_2$ Isotopomers

	^{132}Xe−$(H_2O)_2$	^{131}Xe−$(H_2O)_2$[a]	^{129}Xe−$(H_2O)_2$
	rotational constants/MHz		
A	6267.5930 (6)	6267.6063 (5)	6267.6342 (7)
B	1394.3165 (2)	1396.5752 (4)	1401.2012 (2)
C	1137.1418 (1)	1137.6434 (1)	1141.7196 (1)
	centrifugal distortion constants/kHz		
D_J	5.320 (5)	5.33 (1)	5.374 (5)
D_{JK}	49.15 (4)	49.25 (9)	49.37 (7)
D_K	−0.45 (12)	0.0	−0.61 (12)
d_1	−1.088 (4)	−1.095 (8)	−1.100 (4)
d_2	−0.249 (7)	0.0	-0.283 (15)
	^{131}Xe quadrupole coupling constants/MHz		
χ_{aa}		2.108 (2)	
χ_{bb}		−1.300 (3)	
χ_{cc}		−0.808 (3)	
$\lvert\chi_{ab}\rvert$		8.446(29)	
	standard deviation/kHz		
σ/kHz	1.5	2.5	1.5

[a] D_K and d_2 were fixed at 0.0 for the ^{131}Xe−$(H_2O)_2$ isotopomer.

2. ^{131}Xe−$(H_2O)_2$. The rotational spectra of ^{131}Xe−$(H_2O)_2$ are complicated by the nuclear quadrupole hyperfine structures due to the presence of the ^{131}Xe ($I = {}^3/_2$) nucleus. The hyperfine structures of four *a*-type and seven *b*-type transitions were partially resolved. Figure 1 gives an example spectrum to demonstrate the signal-to-noise ratio and resolution achieved. All measured frequencies are summarized in Table S2 of the Supporting Information and were used to fit the rotational, centrifugal distortion, and ^{131}Xe nuclear quadrupole coupling

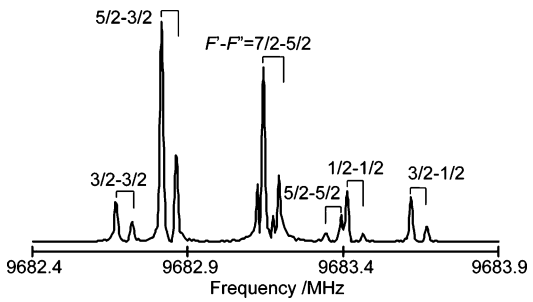

Figure 1. Composite spectrum of the $J_{KaKc} = 2_{12} - 1_{01}$ transition of the ^{131}Xe−$(H_2O)_2$ isotopomer. A total of 2000 averaging cycles was used to record the spectrum.

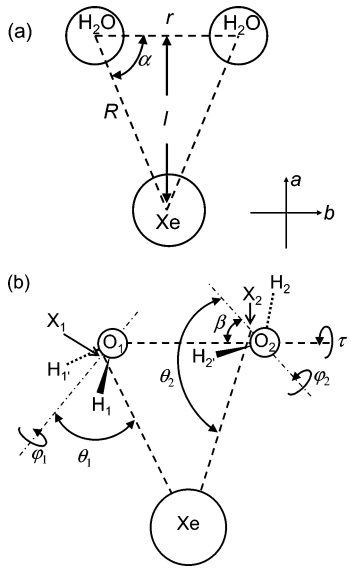

Figure 2. Definition of structural parameters for the Xe−$(H_2O)_2$ complex. The *a*- and *b*-axes are the principal inertial axes of the complex. The parameters defined in (a) were used for the structural analysis: r = c.m.(H_2O)−c.m.(H_2O) distance, R = Xe−c.m.(H_2O) distance, l = Xe−c.m.$[(H_2O)_2]$ distance, and $\alpha = \angle$[Xe−c.m.(H_2O)−c.m.(H_2O)]. Additional parameters defined in (b) were used in the ^{131}Xe nuclear quadrupole hyperfine structure analysis: $\theta_1 = 180° - \angle(Xe-X_1-O_1)$, $\varphi_1 = \angle(Xe-O_1-X_1-H_1)$, $\theta_2 = 180° - \angle(Xe-X_2-O_2)$, $\varphi_2 = \angle(Xe-O_2-X_2-H_2)$, $\beta = \angle(O_1-O_2-X_2)$, and $\tau = \angle(X_1-O_1-O_2-X_2)$.

constants simultaneously. The determined spectroscopic constants are given in Table 1. Inclusion of the off-diagonal nuclear quadrupole coupling constant χ_{ab} was necessary for the hyperfine analysis because of perturbations caused by the near degeneracy of the 1_{10} and 2_{02} energy levels (~80 MHz energy difference). The contribution from χ_{ab} to each transition frequency was calculated using Pickett's SPCAT program[14] and is included in Table S2 of the Supporting Information. This contribution was found to be significant (30−65 kHz) for transitions involving the 1_{10} and 2_{02} energy levels, while it was negligible for other transitions.

Structural Analysis

The rotational constants of Xe−$(H_2O)_2$ can be used to estimate the structural parameters of the trimer, such as the Xe−c.m.(H_2O) distance, R, and the c.m.(H_2O)−c.m.(H_2O) distance, r, by treating the water molecules as spheres. The A rotational constant of the Xe−$(H_2O)_2$ trimer (6267.6 MHz) is rather close to the $(B+C)/2$ value of the water dimer (6160.7 MHz),[15] which is consistent with the initially assumed isosceles triangular structure. The small inertial defect (Δ = 1.34 amu Å^2) and relatively small quartic centrifugal distortion constants of ^{132}Xe−$(H_2O)_2$ (see Table 1) suggest that a semirigid model can be applied here, with the following inertial equations

$$I_a = \frac{1}{2} mr^2 \quad (1)$$

$$I_b = \mu l^2 \quad (2)$$

$$I_c = \mu l^2 + \frac{1}{2} mr^2 \quad (3)$$

Here, m is the mass of water, $\mu = m_{Xe} m_{(H_2O)_2}/(m_{Xe} + m_{(H_2O)_2})$, and l is the distance between Xe and the c.m of the water dimer [see Figure 2a]. By solving eqs 1 and 2, we obtained r = 2.992 Å and l = 3.579 Å. From these values, the Xe−c.m.(H_2O) distance R was calculated to be 3.879 Å. The angle α between the Xe−c.m.(H_2O) bond and the c.m.(H_2O)−c.m.(H_2O) bond was obtained to be 67.3°. Compared with the corresponding separations in the Xe−H_2O dimer (3.949 Å),[9] the Xe−c.m.(H_2O) distance R is shortened by 0.07 Å in the trimer. In other instances, for example, the rare gas trimers Ne_2−Kr and Ne_2−Xe,[16] the van der Waals bond distances were found to be longer than in the corresponding dimers due to the repulsive, nonadditive triple-dipole dispersion term. A possible explanation for the shrinkage of the Xe−H_2O bond in the Xe−$(H_2O)_2$ trimer is that a water molecule induces dipole moments on Xe and the other water molecule with the result of an attractive, nonadditive electrostatic interaction. The shrinkage of the Xe−H_2O bond indicates that this attractive interaction affects the Xe−H_2O bond length more than the repulsive triple-dipole dispersion term. This electrostatic interaction is expected to be less pronounced between two water molecules because the nonpolar Xe atom cannot induce a significant dipole moment on water molecules. This also is consistent with the observation that a slightly longer H_2O−H_2O bond length was found in the Xe−$(H_2O)_2$ trimer (2.992 Å) compared to the water dimer (2.98 Å).[17]

TABLE 2: Vibrational Frequencies and Force Constants of Xe−$(H_2O)_2$ from a Harmonic Force Field Analysis[a]

vibrational force constants	vibrational frequencies
F_{11} = 10.76 (7) N m^{-1}	ν_1 = 143.2 cm^{-1}
F_{22} = 1.489 (4) N m^{-1}	ν_2 = 38.5 cm^{-1}
F_{33} = 1.508 (4) N m^{-1}	ν_3 = 38.8 cm^{-1}

[a] All off-diagonal force constants were fixed at zero during the fit procedure.

Harmonic Force Field Analysis

The ASYM20PC program of Hedberg and Mills[18] was used to perform a harmonic force field analysis for the Xe−$(H_2O)_2$ complex to extract information about van der Waals vibrational frequencies and corresponding force constants. We considered the water molecules as pseudoatoms, and C_s point group symmetry was used for the analysis. Three vibrational modes were considered for this complex, i.e., the H_2O−H_2O stretch (ν_1) and the symmetric (ν_2) and asymmetric (ν_3) H_2O−Xe−H_2O stretches. The force constant matrix $\boldsymbol{F}$ is then a 3 × 3 matrix with diagonal force constants F_{11}, F_{22}, and F_{33} corresponding to the three vibrational modes, respectively. The quartic centrifugal distortion constants of the ^{132}Xe−$(H_2O)_2$, ^{131}Xe−$(H_2O)_2$, and ^{129}Xe−$(H_2O)_2$ isotopomers listed in Table 1 were used to refine the diagonal force constants. All off-diagonal terms were fixed at zero during the fit. The corresponding harmonic frequencies were then calculated from the obtained force constants using Wilson's GF matrix method.[19] This analysis could reproduce the D_J, D_{JK}, and d_1, d_2 centrifugal distortion constants within 5% of the experimental values, especially good agreement was found for the D_J and D_{JK} constants. The D_K constants deviate by up to 32% from the experimental values, but the deviations are on the same order of the magnitude as the experimental uncertainties. All obtained force constants and harmonic frequencies are summarized in Table 2. A comparison of the observed and calculated centrifugal distortion constants is provided in Table S3 of the Supporting Information. The values of the F_{22} (1.489 N m^{-1}) and F_{33} (1.508 N m^{-1}) force constants are 30−40% larger than that of the Xe−H_2O stretching force constant (1.134 N m^{-1}) in the dimer, while the F_{11} value, 10.76 N m^{-1}, is nearly identical to the corre-

sponding value (10.8 N m^{-1}) of the water dimer.[15,17] The increase of the Xe−H_2O stretching force constant in going from the dimer to the trimer can also be attributed to an attractive electrostatic interaction as a result of the induced dipoles. This attractive force lowers the Xe−H_2O binding potential and leads to a stronger van der Waals bond. The H_2O−H_2O stretch force constant is less affected because of the smaller nonadditive electrostatic effect caused by the nonpolar Xe atom.

^{131}Xe Nuclear Quadrupole Coupling Constants

The spherically symmetric charge distribution of a free xenon atom is distorted by the presence of two water molecules, leading to nonzero ^{131}Xe nuclear quadrupole coupling constants. This provides an opportunity to extract information about the electronic charge distribution of the xenon atom. The main contribution to the electric field gradient at the xenon nucleus comes from the electric multipole moments of H_2O. It is therefore sensitive to the H_2O orientations, and we were able to obtain dynamical information about the internal angular coordinates of the Xe−$(H_2O)_2$ complex and to determine effective orientations of the two H_2O molecules from the experimental nuclear quadrupole coupling constants. For example, the surprisingly large value of the off-diagonal constant χ_{ab} (±8.446 MHz) is an indication of high asymmetry of the xenon electron distribution with respect to the *ac* and *bc* inertial planes. The two H_2O molecules adopt distinct effective orientations relative to the xenon atom and, as a result, contribute differently to the electric field gradient at the xenon nucleus. From the experimentally determined constants, we were able to calculate the components of the principal quadrupole coupling axis system ($a'b'c'$). The resulting $\chi_{a'a'}$, $\chi_{b'b'}$, and $\chi_{c'c'}$ values are 9.020, −8.212, and −0.808 MHz, respectively. The c'-axis coincides with inertial *c*-axis, and the a'- and b'-axes are rotated by 39.3° from the *a* and *b* inertial axes. The nuclear quadrupole coupling constants along each Xe−c.m.(H_2O) bond were also determined by projecting the principal axis components onto the corresponding Xe−c.m.(H_2O) intermolecular axis, and the obtained values are 7.614 and −4.414 MHz, respectively. The absolute values are larger by an order of magnitude than the corresponding constant of the ^{131}Xe−H_2O dimer ($\chi_{aa} = -0.445$ MHz),[9] which indicates that the water internal motions are largely hindered in the trimer by interaction with a second water molecule. This also provides evidence for the sensitivity of the electronic structure of the Xe atom upon its surrounding, and the nuclear quadrupole coupling constants can be used to identify the number of surrounding water molecules and their relative positions.

To obtain further information about the effective H_2O orientations, we predicted the nuclear quadrupole coupling constants for different H_2O orientations to search for a geometry, which can reproduce the experimental nuclear quadrupole coupling constants. In these calculations, the water monomers were kept rigid at the experimental structure.[20] The intermolecular structural parameters, *r*, *R*, and α, were fixed at the values estimated from the rotational constants. Six additional angles are necessary to describe the water orientations, as defined in Figure 2b. θ_1(180° − ∠Xe−X_1−O_1), φ_1(∠Xe−O_1−X_1−H_1), θ_2(180° − ∠Xe−X_2−O_2), and φ_2(∠Xe−O_2−X_2−H_2) describe the orientations of two water molecules, relative to the xenon atom. X_1 and X_2 are the c.m. of the two water molecules, respectively. β (∠O_1−O_2−X_2) and τ (∠X_1−O_1−O_2−X_2) are used to define the relative orientations of two water molecules.

We first calculated the electric field gradient tensor at the Xe nucleus contributed by the electric multiple moments of each H_2O molecule individually. In each calculation, we considered the dipole moment (μ = 1.8546 D, ref 21) and quadrupole moment ($Q_{xx} = -2.50$ D Å, $Q_{yy} = 2.63$ D Å, and $Q_{zz} = -0.13$ D Å, ref 22) of H_2O and neglected the higher order electric moments. We reproduced the dipole[21] and quadrupole[22] moments of H_2O by four point charges of equal magnitude, two positive and two negative. The positive charges lie near the two H atoms, and the negative charges sit on the two sides of the H_2O plane and near the O atom.[23] The electric field gradient tensor at the Xe nucleus was then calculated as a summation over contributions from the four point charges.[24]

The determined two electric field gradient tensors contributed by two H_2O molecules were summed up to generate the corresponding tensor in the Xe−$(H_2O)_2$ complex. This tensor was then used to obtain the ^{131}Xe nuclear quadrupole coupling constants,[25] according to eq 4. The experimental ^{131}Xe nuclear quadrupole coupling constants of the Ne_2−^{131}Xe complex, χ_{aa} (0.564 MHz) and χ_{bb} (−0.256 MHz),[16] were used to approximate the effect of the dispersion interaction.

$$\begin{pmatrix} \chi_{aa} & \chi_{ab} & \chi_{ac} \\ \chi_{ab} & \chi_{bb} & \chi_{bc} \\ \chi_{ac} & \chi_{bc} & \chi_{cc} \end{pmatrix} = -\frac{e(1-\gamma)Q_{\mathrm{Xe}}}{h} \begin{pmatrix} q_{aa} & q_{ab} & q_{ac} \\ q_{ab} & q_{bb} & q_{bc} \\ q_{ac} & q_{bc} & q_{cc} \end{pmatrix} + \begin{pmatrix} 0.564 & 0 & 0 \\ 0 & -0.256 & 0 \\ 0 & 0 & -0.308 \end{pmatrix} \quad (4)$$

Here, q_{ij} and χ_{ij} ($i, j = a, b, c$) are the components of the electric field gradient and nuclear quadrupole coupling tensor, respectively, in the inertial axis system, $Q_{\mathrm{Xe}} = -0.12$ b is the ^{131}Xe nuclear quadrupole moment,[26] and $\gamma = -152$ is the Sternheimer shielding factor.[25]

The best agreement between the calculated and experimental constants was found in the structure with $\theta_1 = 148°$, $\varphi_1 = 90°$, $\theta_2 = 43°$, $\varphi_2 = 41°$, $\beta = 30°$, and $\tau = 151°$. The calculated values are $\chi_{aa} = 2.858$ MHz, $\chi_{bb} = -1.045$ MHz, $\chi_{ab} = 7.694$ MHz, which differ from the experimental ones by 0.7, 0.3, and −0.7 MHz, respectively. It is interesting to note that the χ_{ab} value is more sensitive to the dipole moment of H_2O than χ_{aa} and χ_{bb} values. For example, if the dipole moment increases by 10%, the χ_{ab} value (8.347 MHz) increases by 0.65 MHz, while the changes of χ_{aa} (2.941 MHz) and χ_{bb} values (−1.096 MHz) are 0.1 MHz. This improvement of the χ_{ab} value without too large an effect on χ_{aa} and χ_{bb} could be viewed as further evidence of the large three-body effect from the nonadditive electrostatic interactions as a result of induced dipoles, which supports what we suggested in the structural and harmonic force field analyses above.

Because of an insufficient description of the dispersion interactions, three-body effects, and large amplitude vibrational motions of the complex, this calculation cannot be viewed as a highly accurate structure determination. However, this still can be regarded as a reasonable first approximation to generate a picture of the electric field gradient at the Xe nucleus and to predict the H_2O orientation within the complex. A more accurate model describing the intermolecular interactions in the complex will improve the structure calculation.

To rationalize the determined effective structure, we performed a complete geometry optimization at the level of second-order Møller−Plesset perturbation theory (MP2)[27] using the GAUSSIAN03 package of ab initio programs.[28] The aug-cc-pVQZ-PP[29] basis set was used for the Xe atom, aug-cc-pVTZ[30] for the O atoms, and 6-311++G(d,p)[31] for the H atoms. Two minimum-energy configurations were located (see Figure 3), and their structural parameters are listed in the Table S4 of the

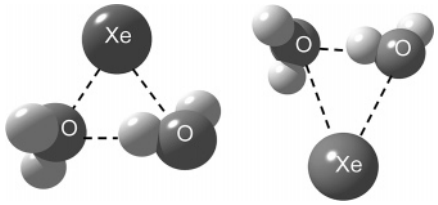

Figure 3. Geometries of Minimum I (left) and Minimum II (right) of the Xe−$(H_2O)_2$ trimer optimized at the MP2 level of theory. The unlabeled elements are H atoms.

Supporting Information. Their minimum natures were confirmed by the absence of imaginary frequencies in the harmonic frequency calculation. Both these configurations have triangular geometries, which are consistent with the experimental results. In Minimum I, the Xe atom approaches the hydrogen side of the proton donor water molecule and the backside of the acceptor water. The situation is reversed in Minimum II (see Figure 3). The remaining structural parameters, other than the position of the Xe atom, of these two minima agree with each other and are consistent with the effective, experimental structure obtained from structural and nuclear quadrupole hyperfine analyses considering large amplitude vibrational and internal rotation motion. The experimental position of the xenon atom is closer to Minimum I, which has a higher zero-point corrected binding energy than Minimum II, by ∼1 kJ/mol (see Table S5 of the Supporting Information). This suggests that the effective structure is highly averaged over the internal angular coordinates of the complex as a result of a rather delocalized ground state wavefunction. The van der Waals stretching frequencies from the harmonic force field analysis are within the same order of magnitude as the corresponding ab initio frequencies (see Table S5 of the Supporting Information).

Conclusions

Rotational spectra of the Xe−$(H_2O)_2$ complex were recorded with a Fourier transform microwave spectrometer. The spectroscopic results provide detailed information about structure and vibrational dynamics of the complex. The analyses suggest that an attractive electrostatic interaction as a result of induced dipole moments makes crucial contributions to non-additive three-body effects. Nuclear quadrupole hyperfine structures due to the ^{131}Xe ($I = {}^3/_2$) nucleus were detected and provide detailed insight into the electronic structure of the xenon atom. The coupling constants are therefore an exquisite probe of the electrostatic environment of the Xe atom. In particular, the large value of the off-diagonal nuclear quadrupole coupling constant χ_{ab} provides evidence for different contributions to the electronic environment of the Xe nucleus by the two H_2O molecules. An effective structure of the trimer, based on reproducing the experimental ^{131}Xe nuclear quadrupole coupling constants, is supported by ab initio calculations. The detailed insight provided into the variations of structure and vibrational dynamics in going from the Xe−H_2O dimer to the Xe−$(H_2O)_2$ trimer constitutes a step toward the understanding of "macroscopic" Xe−water surroundings interactions. The interpretation of the ^{131}Xe nuclear quadrupole coupling constants can shed light on the effect of the surrounding water distribution upon the electronic structure of the xenon atom. This work is fundamental to the goal of achieving molecular level interpretations of xenon shielding responses and macroscopic phenomena observed in Xe NMR experiments.

Acknowledgment. This work was funded by the Natural Sciences and Engineering Research Council of Canada. We thank D. Bremm and Z. Su for helpful discussions and suggestions. We thank the anonymous referee for valuable suggestions regarding the calculation of the nuclear quadrupole coupling constants.

Supporting Information Available: Tables with measured transition frequencies, calculated quartic centrifugal distortion constants from harmonic force field analysis, and ab initio data. This material is available free of charge via the Internet at http://pubs.acs.org.

References and Notes

(1) Navon, G.; Song, Y.−Q.; Room, T.; Appelt, S.; Taylor, R. E.; Pines, A. *Science* **1996**, *271*, 1848.

(2) Cherubini, A.; Bifone, A. *Prog. Nucl. Magn. Reson. Spectrosc.* **2003**, *42*, 1.

(3) Goodson, B. M. *J. Magn. Reson.* **2002**, *155*, 157.

(4) Albert, M. S.; Cates, G. D.; Driehuys, B.; Happer, W.; Saam, B.; Springer, C. S., Jr.; Wishnia, A. *Nature* **1994**, *370*, 199.

(5) Ugurbil, K.; Adriany, G.; Andersen, P.; Chen, W.; Gruetter, R.; Hu, X.; Merkle, H.; Kim, D. -S.; Kim, S. -G.; Strupp, J.; Zhu, X. H.; Ogawa, S. *Annu. Rev. Biomed. Eng.* **2000**, *2*, 633.

(6) Huber, G.; Brotin, T.; Dubois, L.; Desvaux, H.; Dutasta, J.−P.; Berthault, P. *J. Am. Chem. Soc.* **2006**, *128*, 6239.

(7) Jameson, C. J.; Sears, D. N.; Murad, S. *J. Chem. Phys.* **2004**, *121*, 9581.

(8) Stueber, D.; Jameson, C. J. *J. Chem. Phys.* **2004**, *120*, 1560.

(9) Wen, Q.; Jäger, W. *J. Phys. Chem. A* **2006**, *110*, 7560.

(10) Arunan, E.; Emilsson, T.; Gutowsky, H. S. *J. Chem. Phys.* **2002**, *116*, 4886.

(11) Arunan, E.; Emilsson, T.; Gutowsky, H. S. *J. Am. Chem. Soc.* **1994**, *116*, 8418.

(12) Xu, Y.; Jäger, W. *J. Chem. Phys.* **1997**, *106*, 7968.

(13) Fraser, G. T.; Lovas, F. J.; Suenram, R. D.; Matsumura, K. *J. Mol. Spectrosc.* **1990**, *144*, 97.

(14) Pickett, H. M. *J. Mol. Spectrosc.* **1991**, *148*, 371.

(15) Dyke, T. R.; Mack, K. M.; Muenter, J. S. *J. Chem. Phys.* **1977**, *66*, 498.

(16) Xu, Y.; Jäger, W.; Gerry, M. C. L. *J. Chem. Phys.* **1994**, *100*, 4171.

(17) Lovas, F. J.; Zobov, N.; Fraser, G. T.; Suenram, R. D. *J. Mol. Spectrosc.* **1995**, *171*, 189.

(18) Hedberg, L.; Mills, I. M. *J. Mol. Spectrosc.* **1993**, *160*, 117.

(19) Kivelson, D.; Wilson, E. B., Jr. *J. Chem. Phys.* **1953**, *21*, 1229.

(20) Cook, R. L.; De Lucia, F. C.; Helminger, P. *J. Mol. Spectrosc.* **1974**, *53*, 62.

(21) Dyke, T. R.; Muenter, J. S. *J. Chem. Phys.* **1973**, *59*, 3125.

(22) Verhoeven, J.; Dymanus, A. *J. Chem. Phys.* **1970**, *52*, 3222.

(23) Stone, A. J. *The Theory of Intermolecular Forces*; Clarendon: Oxford, 1996.

(24) Gray, C. G.; Gubbins, K. E. *Theory of Molecular Fluids*; Clarendon: Oxford, 1984; Vol. 1.

(25) Campbell, E. J.; Buxton, L. W.; Keenan, M. R.; Flygare, W. H. *Phys. Rev. A* **1981**, *24*, 812.

(26) Faust, W. L.; McDermott, M. N. *Phys. Rev.* **1961**, *123*, 198.

(27) Binkley, J. S.; Pople, J. A. *Int. J. Quantum Chem.* **1975**, *9*, 229.

(28) Frisch, M. J.; Trucks, G. W.; Schlegel, H. B.; Scuseria, G. E.; Robb, M. A.; Cheeseman, J. R.; Montgomery, J. A., Jr.; Vreven, T.; Kudin, K. N.; Burant, J. C.; Millam, J. M.; Iyengar, S. S.; Tomasi, J.; Barone, V.; Mennucci, B.; Cossi, M.; Scalmani, G.; Rega, N.; Petersson, G. A.; Nakatsuji, H.; Hada, M.; Ehara, M.; Toyota, K.; Fukuda, R.; Hasegawa, J.; Ishida, M.; Nakajima, T.; Honda, Y.; Kitao, O.; Nakai, H.; Klene, M.; Li, X.; Knox, J. E.; Hratchian, H. P.; Cross, J. B.; Bakken, V.; Adamo, C.; Jaramillo, J.; Gomperts, R.; Stratmann, R. E.; Yazyev, O.; Austin, A. J.; Cammi, R.; Pomelli, C.; Ochterski, J. W.; Ayala, P. Y.; Morokuma, K.; Voth, G. A.; Salvador, P.; Dannenberg, J. J.; Zakrzewski, V. G.; Dapprich, S.; Daniels, A. D.; Strain, M. C.; Farkas, O.; Malick, D. K.; Rabuck, A. D.; Raghavachari, K.; Foresman, J. B.; Ortiz, J. V.; Cui, Q.; Baboul, A. G.; Clifford, S.; Cioslowski, J.; Stefanov, B. B.; Liu, G.; Liashenko, A.; Piskorz, P.; Komaromi, I.; Martin, R. L.; Fox, D. J.; Keith, T.; Al-Laham, M. A.; Peng, C. Y.; Nanayakkara, A.; Challacombe, M.; Gill, P. M. W.; Johnson, B.; Chen, W.; Wong, M. W.; Gonzalez, C.; Pople, J. A. *Gaussian 03*, revision B.01; Gaussian, Inc.: Pittsburgh, PA, 2003.

(29) Peterson, K. A.; Figgen, D.; Goll, E.; Stoll, H.; Dolg, M. *J. Chem. Phys.* **2003**, *119*, 11113.

(30) Dunning, T. H., Jr. *J. Chem. Phys.* **1989**, *90*, 1007.

(31) Krishman, R.; Binkley, J. S.; Seeger. R.; Pople, J. A. *J. Chem. Phys.* **1980**, *72*, 650.